Robust and flexible random lasers using perovskite quantum dots coated Nickel foam for speckle-free laser imaging

*Wei Gao, Ting Wang, Jiangtao Xu, Ping Zeng, Wenfei Zhang, Yunduo Yao, Changsheng Chen, Mingjie Li, Siu Fung Yu**

Wei Gao, Yunduo Yao, Changsheng Chen, Dr. Mingjie Li, Prof. Siu Fung Yu
Department of Applied Physics, The Hong Kong Polytechnic University, Kowloon, Hong Kong, China
E-mail: sfyu21@hotmail.com

Wei Gao, Prof. Siu Fung Yu
Shenzhen Research Institute, The Hong Kong Polytechnic University, Shenzhen 518060, China

Dr. Ting Wang
College of Materials and Chemistry & Chemical Engineering, Chengdu University of Technology, Chengdu 610059, China

Jiangtao Xu
Institute of Textiles and Clothing, The Hong Kong Polytechnic University, Kowloon, Hong Kong, China

Ping Zeng
State Key Laboratory of Chemical Biology and Drug Discovery and Department of Applied Biology and Chemical Technology, The Hong Kong Polytechnic University, Kowloon, Hong Kong, China

Dr. Wenfei Zhang
Shenzhen Key Laboratory of Laser Engineering, College of Physics and Optoelectronic Engineering, Shenzhen University, Shenzhen 518060, China

Keywords: perovskite quantum dots, Ni porous foams, incoherent random lasing, flexible lasers, two-photon excitation

The advantage of using flexible metallic structures as the substrate of flexible lasers over plastic materials is its strong mechanical strength and high thermal conductivity. Here, we propose to deposit $CsPbBr_3$ perovskite quantum dots onto Ni porous foam for the realization of flexible lasers. Under two-photon 800 nm excitation at room temperature, we observe incoherent random lasing emission at ~537 nm. By external deformation of the Ni porous foam, incoherent random lasing can be tuned to amplified spontaneous emission as well as the corresponding lasing threshold can be controlled. More importantly, we have demonstrated that the laser is robust to intensive bending (>1000 bending cycles) with minimum effect on the lasing intensity.

This flexible laser is also shown to be an ideal light source to produce a 'speckle' free micro-image.

1. Introduction

Recently, extensive investigations have been concentrated on the realization of lasers on the plastic substrate due to their mechanical flexible characteristics suitable for the development of flexible optoelectronic systems.[1-5] For example, the deposition of ZnO nanoparticle embedded ZnO thin film on polycarbonate plastic substrate is proposed to realize flexible inorganic random lasers.[6] Organic lasers using solvent-free fluidic organic semiconductors as the gain medium, and highly flexible corrugated polymeric patterns and flexible polyurethane acrylate films as the resonator have also achieved mechanically single-mode tunable lasers.[7] Furthermore, organic dye spin-coated on a polyethylene terephthalate substrate embedded with silver nanoprisms has fabricated flexible random lasers with a high degree of wavelength tunability over 15 nm through the influence of localized surface plasmon and random scattering under mechanical bending.[2] On the other hand, using organic polymers has shown the possibility to obtain mechanical flexibility and lightweight substrateless organic lasers that can be deposited on any surface.[8] Spin coating of strong adhesive perovskite thin films on flexible polyimide substrates have also obtained flexible random lasers with the control of excitation threshold through mechanical bending.[9] Alternatively, a flexible gain medium - ZnO-enriched cellulose acetate fiber matrix doped with silver nanoparticles is fabricated as the flexible random cavities to realize flexible lasers.[10] These results verify the possibilities to fabricate functional flexible lasers which are the necessary components for the future development of flexible optoelectronic systems. Nevertheless, it is preferred to realize lasers on flexible metallic substrates, which have high thermal conductivity to suppress overheating at high-power operation (**Figure S1**), to obtain better optical performance. To the best of our knowledge, there is no report on the fabrication of lasers on flexible metallic substrates.

Metal halides perovskites quantum dots (PQDs) have been recognized as optical gain materials over their bulk counterparts due to their insensitivity to oxidization and moisture environment with lower thresholds.[11-14] Besides, the influence of quantum size effects and the use of colloidal structure can easily tune the energy bandgap as well as can enhance the emission intensity of the PQDs.[15-16] The corresponding surface chemistry can also be modified to enable them to disperse into a variety of solvents and matrices, and even integrated into various devices through their strong adhesive performance.[17-19] Recently, all-inorganic $CsPbX_3$ (X=Cl, Br, I) PQDs[20] with highly efficient luminescence were found that they are suitable to be utilized as laser gain materials.[21] More importantly, the combination of optimized solvent engineering processes with PQDs facilitates the synthesis of high-quality solution-processed perovskite thin films on flexible substrates at low cost.[22-23] Therefore, metal halides PQDs are a potential laser gain medium for the fabrication of flexible lasers.

In this study, we propose the use of 1) Ni porous foam (i.e. which has a 3D heat-conductive metallic structure of voids that can endure serious deformation) as the laser substrate and 2) $CsPbBr_3$ PQDs as the gain medium to realize lasers on flexible metallic substrates. Due to the strong light scattering capability of the voids of the Ni foam and the excellent optical gain properties of $CsPbBr_3$ PQDs, we demonstrated incoherent random lasing from the $CsPbBr_3$ PQDs coated Ni porous foam under optical excitation at room temperature. Furthermore, the emission characteristics of the flexible lasers can be tuned by controlling the surface morphologies of the Ni foam through deformation. It is also shown that the corresponding emission intensity is robust to extensive bending. On the other hand, due to the low spatial coherent characteristics of the flexible lasers, it is shown to be an ideal light source to produce high-quality micro images. Hence, our proposed flexible and durable lasers are a potential high-

performance speckle-free light source for the future application of flexible optoelectronic systems.

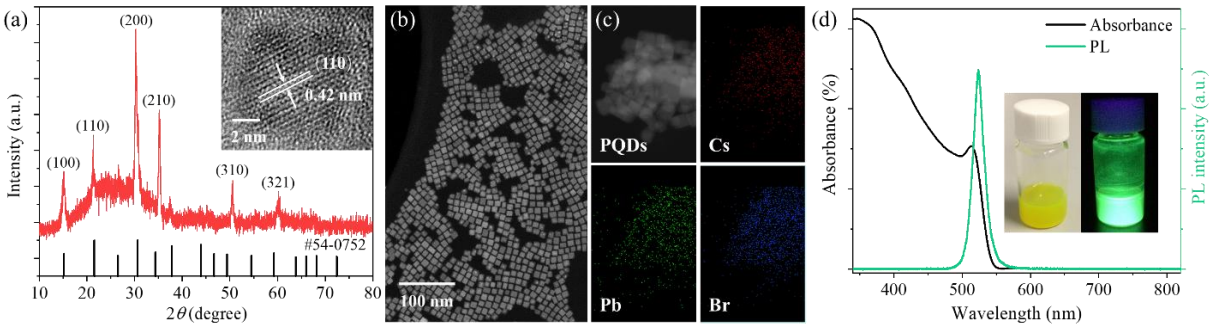

Figure 1. Physical characteristics of $CsPbBr_3$ PQDs. (a) XRD pattern of $CsPbBr_3$ PQDs film on the glass slide and standard card (PDF #54-0752). The inserted image shows the HR-TEM image of a $CsPbBr_3$ PQD. (b) STEM micrograph of $CsPbBr_3$ PQDs. (c) EDX elemental mapping images of $CsPbBr_3$ PQDs. (d) Absorption and photoluminescence emission spectra of the $CsPbBr_3$ PQDs and the inset of (d) shows the photos of the $CsPbBr_3$ PQDs with and without UV light excitation.

2. Results and discussion

2.1. Synthesis and characteristics of $CsPbBr_3$ PQDs

Figure 1a presents the X-ray diffraction (XRD) pattern of the $CsPbBr_3$ PQDs. The pattern matches with the standard cubic crystal structure of $CsPbBr_3$ (PDF #54-0752). High-resolution transmission electron microscopy (HR-TEM) image of a $CsPbBr_3$ PQD given in the inset of Figure 1a has shown that the corresponding nanocrystal length and lattice spacing (110) are equal to ~8 and 0.42 nm respectively. Hence, it is verified that the $CsPbBr_3$ PQDs are in the cubic phase. Scanning transmission electron microscopy (STEM) image of the monodisperse PQDs is also shown in Figure 1b. It is demonstrated that the $CsPbBr_3$ PQDs fabricated by the solution-phase synthesis have a uniform size distribution. Moreover, energy-dispersive X-ray (EDX) elemental mapping images of $CsPbBr_3$ PQDs are given in Figure 1c. Cs, Pb and Br elements are found to be homogeneously distributed over the entire volume which further confirms that the high-crystal-quality cubic phase PQDs were successfully synthesized. Figure 1d shows the optical characteristics of the $CsPbBr_3$ PQDs at room temperature. The

photoluminescence (PL) quantum yield of the $CsPbBr_3$ PQDs dispersed in toluene was found to be ~96%.

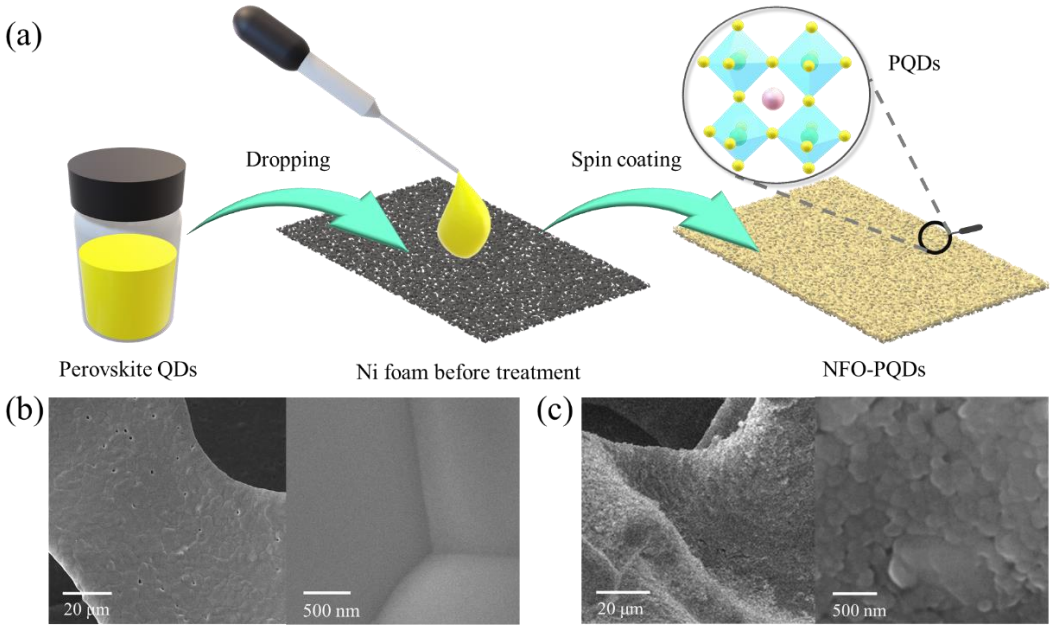

Figure 2. (a) Fabrication process of the Ni foam coated with $CsPbBr_3$ PQDs. SEM images of the surface mesh structure of the Ni foam (b) without and (c) with a coating of $CsPbBr_3$ PQDs.

2.2. Characteristics of Ni foam coated with $CsPbBr_3$ PQDs

Figure 2a describes the fabrication process of Ni porous foam coated with $CsPbBr_3$ PQDs (NFO-PQDs) by using the spin-coating method – few drops of $CsPbBr_3$ PQDs dispersed in toluene is spin-coated onto the surface of Ni foam at a rotational speed of 600 rpm for 10 seconds and then 3000 rpm for 30 seconds, and this procedure is repeated for 3 times. The Ni foam, which can be purchased commercially, has a three-dimensional mesh structure with voids of diameter ~200 μm (**Figures S2** and **S3a**) and thickness of ~300 μm. Figures 2b and 2c show the scanning electron microscope (SEM) images of the Ni foam before and after coating of $CsPbBr_3$ PQDs respectively. It is observed that the entire surface of the mesh structure is covered with $CsPbBr_3$ PQDs with an average thickness of about 200 nm (**Figures S4a** and S4b). Figure S4c shows that the XRD pattern of NFO-PQDs is consistent with the standard card of $CsPbBr_3$ (#54-0752) and Ni (#87-0712), indicating that the $CsPbBr_3$ PQDs was successfully

coated on the Ni foam. The $CsPbBr_3$ PQDs coating, which has an average RMS value of about 50 nm, has a rough surface after coating on the Ni foam. This is due to the surface roughness of the Ni foam. However, this surface roughness has less influence on the emission characteristics of the NFO-PQDs due to the domination of the mesh structure of the Ni foam. The PL quantum yield of the $CsPbBr_3$ PQDs coated on Ni foam is found to be ~53%.

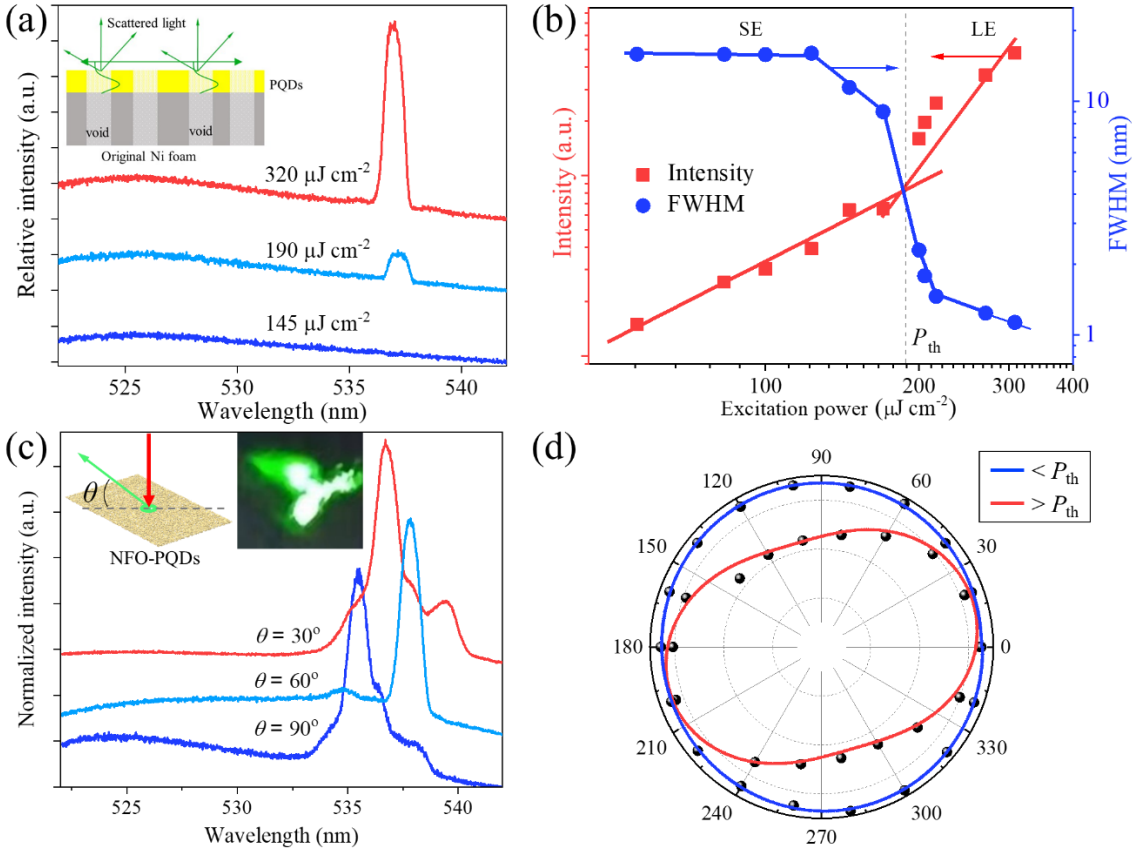

Figure 3. Random lasing characteristics of as-prepared NFO-PQDs. (a) Power-dependent PL spectra. Insert schematically explains how guided modes interact with the NFO-PQDs. (b) Output intensity and linewidth at various excitation power. (c) Observation-angle dependent PL spectra. Insert shows the corresponding near-field profile observed at 30°. (d) Output intensities at different polarization angles for the excitation power below (blue line) and above (red line) P_{th}. The sample is excited by an 800 nm fs laser at room temperature.

2.3. Incoherent random lasing of the as-prepared NFO-PQDs

An 800 nm femtosecond laser was used to examine the PL emission characteristics of the as-prepared NFO-PQDs under two-photon excitation at room temperature. The reason for using 800 nm instead of 400 nm excitation light is its less surface absorption at the surface of Ni so that the PQDs layer can sustain multi-reflection to improve the excitation efficiency of NFO-

PQDs (**Figures S5** and **S6**).[24] **Figure 3a** shows the PL spectra of the as-prepared NFO-PQDs versus the increase of excitation power. A broad emission peak with a peak wavelength at ~525 nm appears in the emission spectra for the excitation power less than 190 μJ cm^{-2}. However, a narrow peak with a peak wavelength at ~537 nm emerges from the broad emission peak for the excitation power equal to or larger than 190 μJ cm^{-2}. The full width at half maximum (FWHM) linewidth of the broad emission peak remains unchanged over the excitation power. Figure 3b plots the corresponding light-light curve and FWHM linewidth of the dominant emission peak. The light-light curve, which shows a kink at a threshold P_{th} ~190 μJ cm^{-2}, indicates the transition from spontaneous emission (SE) to lasing emission (LE). The corresponding FWHM linewidth of the dominant emission peak reduces significantly from ~16 to ~1 nm for the increase of excitation power. Hence, the as-prepared NFO-PQDs demonstrate lasing emission at room temperature and a typical S-shape of light-light curve is not observed. [25] Figure 3c shows the angle-resolved PL spectra of the sample at different observation angles, θ, under high power excitation (i.e. >> P_{th}). It is noted the profile of the PL spectra is different at different elevation angles and the corresponding linewidth is less than 1.5 nm. The inset of Figure 3c presents the near-field emission beam profile of the PL spectra which shows strong light scattering at different angles from the surface of the NFO-PQDs. This is expected as the optical feedback mechanism is direction-dependent inside the volume of NFO-PQDs.[26] Figure 3d plots the polarization characteristics of the as-prepared samples below and above the excitation threshold. For the sample biased below the threshold, the emission light is unpolarized. For the sample excited above the threshold, the emission light is partially polarized. Hence, it is verified that the as-prepared samples support incoherent random lasing at room temperature due to the following reasons: 1) the observation of P_{th} and narrowing of linewidth suggests laser behavior, 2) as the sample has no defined laser cavity, the variation of spectral and spatial profile at different elevation angles suggests the presence of random light scattering inside the NFO-

PQDs, and 3) the observation of partial polarization and the absence of sharp peaks (i.e. linewidth < 0.2 nm) suggest the feedback mechanism is incoherent optical feedback.[27] Furthermore, a linear relationship between $A_{th}^{2/3}$ and $1/P_{th}$ (**Figure S7**) confirms that the confined modes inside the NFO-PQDs exhibit random lasing action where A_{th} is the threshold excitation area.[28]

2.4. Incoherent optical feedback from the mesh structure of the Ni foam

Here, we study the influence of surface morphologies of the Ni foam on the lasing characteristics of NFO-PQDs. We consider the cases for Ni foam under deformation by external compression from horizontal and vertical directions (**Figure S8**). After the deformation of the Ni foam, $CsPbBr_3$ PQDs were spin-coated onto the samples by the same method given in Figure 2a. The PL emission characteristics of the vertical compacted Ni foam coated with $CsPbBr_3$ PQDs are demonstrated in **Figure 4**. Due to the high vertical pressure, the voids of the Ni foam fill up with the material underneath them so that a flatted Ni surface is obtained (Figure S3b). Hence, the spin-coated PQDs layer forms a waveguiding layer on the flat Ni surface with strong optical confinement as shonwn in the inset of Figure 4a. From the studies shown in Figure 4b, the narrowing of emission peak from 15 to 3 nm occurs when the excitation power exceeds a threshold P_{th} ~240 μJ cm^{-2}. However, the profile of the emission spectra is independent of the elevation angle of observation. Similar emission characteristics of PQDs layer spin-coated on a flat Ni film are also observed (**Figure S9**). These phenomena imply that the sample only supports ASE as voids are absent from the surface of the Ni foam to support light scattering. It should be noted that ASE has a slightly higher P_{th} than that of the incoherent random lasing as given in Figure 3 due to the absence of optical scatterers.

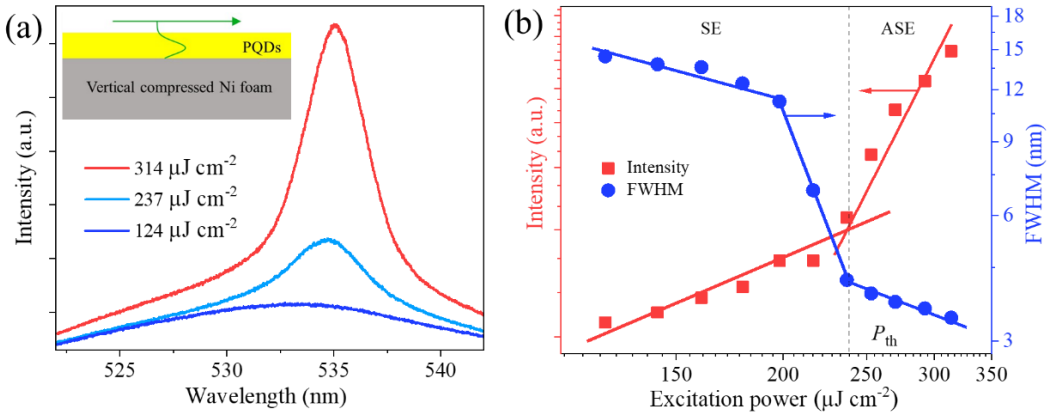

Figure 4. Emission characteristics of NFO-PQDs with vertically compressed Ni foam under 800 nm fs laser excitation at room temperature. (a) Emission PL spectra measured at different excitation power. Insert schematic explains how guided modes interact with the compressed NFO-PQDs. (b) Output intensity and linewidth at various excitation power.

Figure 5 plots the PL emission characteristics of the horizontal compacted Ni foam with the deposition of $CsPbBr_3$ PQDs. In this case, the diameter of the voids is reduced to between 60 and 90 μm. Therefore, the number of voids per unit area is increased compared to that in the original sample as shown in the inset of Figure 5a and Figure S3c. In Figure 5a and 5b, the narrowing of FWHM linewidth (i.e. from 25 to 1 nm) is observed when the excitation power exceeds a threshold P_{th} ~100 μJ cm^{-2}. On the other hand, Figure 5c shows that the angle-resolved PL spectra of the sample at different observation angles, θ, under high power excitation (i.e. >> P_{th}) are different. The corresponding emission light is also partially polarized at the excitation above the threshold (Figure 5d). Therefore, the sample support incoherent random lasing but the corresponding P_{th} is reduced by half compared to that given in Figure 3. The reduction of excitation threshold can be understood by the increase of the number of voids (i.e. number of optical scatterers) per unit area experiences by the optical modes. Previous analysis of random lasers has shown that lasing threshold intensity P_{th} decreased with the light transport length, l_t through the relationship of $P_{th} \propto l_t^{1/2}$.[29] In our NFO-PQDs, the transport length of the scattered light should be roughly equal to the diameter of the voids. As the diameter of voids of the original Ni foam and that after horizontal compression are ~200 and ~70 μm respectively, the value of P_{th} for the horizontal compressed NFO-PQDs should be

reduced by ~2 fold. This is roughly consistent with our measurement of P_{th} shown in Figure 3 and Figure 5.

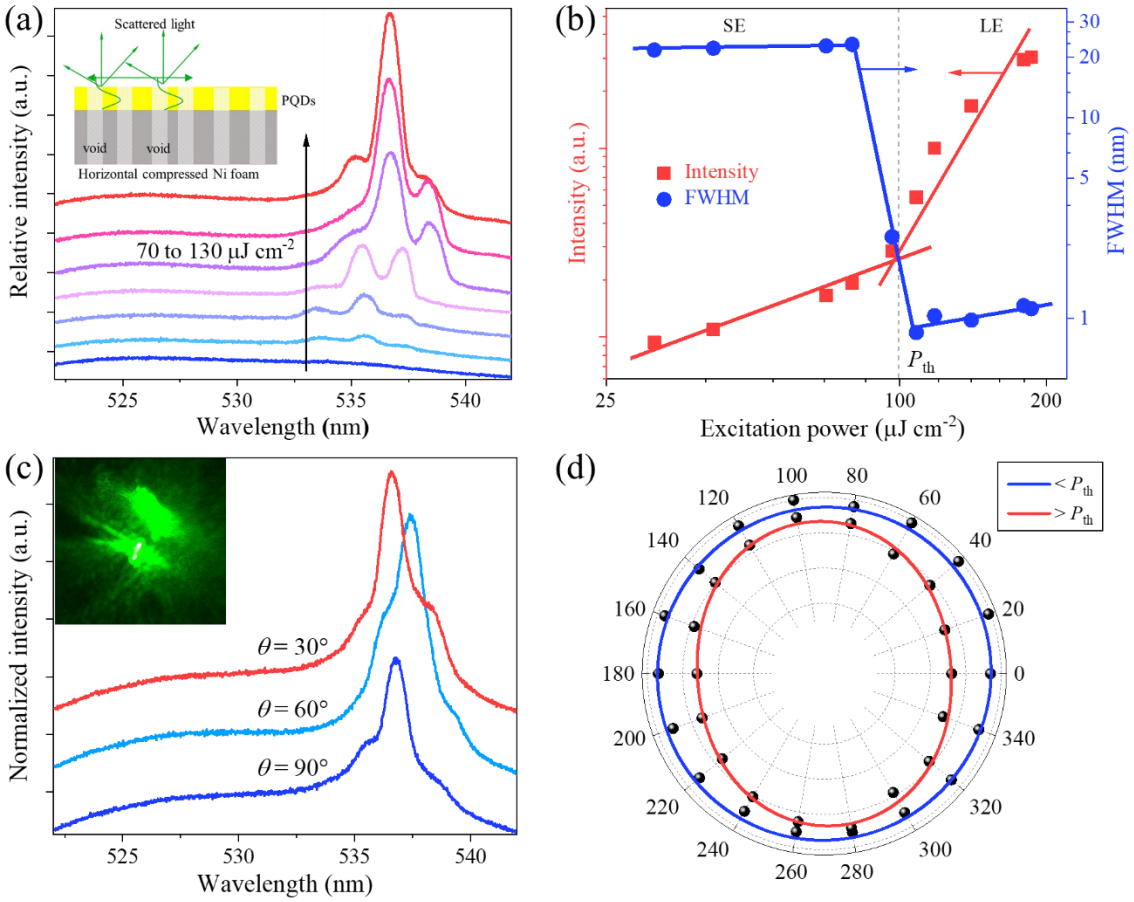

Figure 5. Emission characteristics of NFO-PQDs with a horizontally compressed Ni foam under 800 nm fs laser excitation at room temperature. (a) Emission PL spectra measured at different excitation power. Insert schematic explains how guided modes interact with the compressed NFO-PQDs. (b) Output intensity and linewidth at various excitation power. (c) Emission spectra were detected at different angles for lasing mode. Inset of (c) shows the corresponding near-field profile observed at 30°. (d) Output intensities at different polarization angles for the excitation power below (blue line) and above (red line) P_{th}.

It is noted from Figure 3 to Figure 5 that the dominant emission peak redshifts from ~526 to ~536 nm. The redshift can be attributed to the increase in net optical gain arisen from the propagation of optical modes inside the NFO-PQDs. On the other hand, the redshift may also be related to the aggregation of PQDs (i.e. increase in size) on the Ni foam.[30] However, our investigations have indicated that the redshift only occurs above the excitation threshold so that the presence of NFO-PQDs is the main reason for the observations. In the above experiment, the maximum output power measured from the NFO-PQDs is about 20 μW.

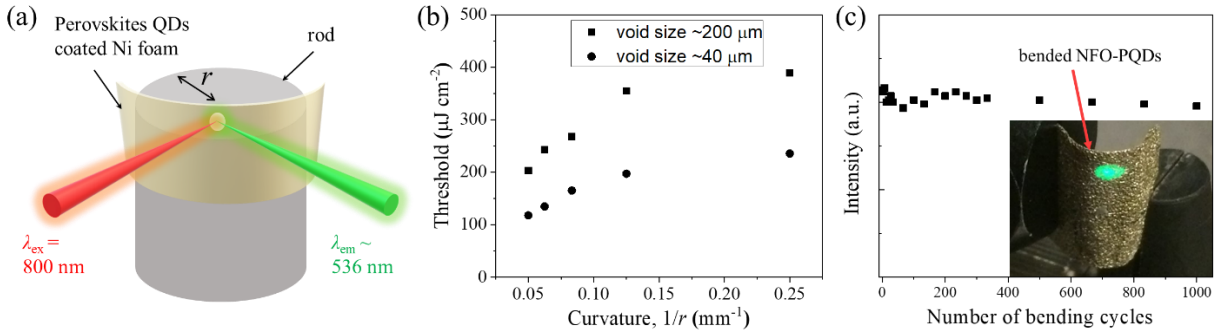

Figure 6. Experiment to measure the bending effect on the emission characteristics of as-prepared NFO-PQDs. (a) Schematic diagram of the experimental setup. (b) A plot of lasing threshold (P_{th}) versus curvature ($1/r$) of the NFO-PQDs with a size of voids equal to 40 and 100 μm. (c) A plot of intensity versus the number of bending cycles. Inset of (c) shows the photo of the experimental setup.

2.5. The stability of flexible NFO-PQDs lasers

Although halide perovskites often react with metals, the $CsPbBr_3$ PQDs show no chemical reaction with the Ni foams. The chemical stability test of the NFO-PQDs was performed for 15 days at room temperature with humidity control. It is found that the emission characteristics of the NFO-PQDs under a constant excitation power remained unchanged (**Figure S10**). Another advantage of using Ni foam as the substrate is its mechanical flexibility. **Figure 6** studies the influence of bending on the emission characteristics of the as-prepared NFO-PQDs. The schematic diagram of the experimental setup is shown in Figure 6a. In the experiment, the NFO-PQDs are bent by sticking the coated Ni foam on a rod with different radius, r, varies from 20 to 4 mm. Emission characteristics of the bent NFO-PQDs with different curvatures (i.e. $1/r$) are measured at room temperature. However, they are not repeatly shown here as they are similar to that shown in Figure 3. Figure 6b plots the corresponding P_{th} versus curvature of the bent NFO-PQDs. It is noted that P_{th} increases with the increase of curvature (i.e. reduce of r).[9] The increase of the threshold can be attributed to the increase of the diameter of the voids due to the bending of the Ni foam. The experiment was repeated with a small porous Ni foam (i.e. void diameter ~40 μm). It is noted that the corresponding P_{th} is lower than that with a large porous size over the range of curvatures as $P_{th} \propto l_t^{1/2}$ and the bending effect is the same for both Ni

foams. Hence, it is verified that the porosities act as scatterers, which provide incoherent optical feedback to the random modes, inside the NFO-PQDs.

The reliability of using NFO-PQDs as flexible lasers under the influence of long-term bending and scratching is an important advantage for practical application. Here, the stability of the lasing characteristics of the NFO-PQDs is studied by measuring the corresponding lasing intensity versus the number of bending cycles. Figure 6c shows the lasing intensity versus the number of bending cycles of an as-prepared NFO-QDs. In the experiment, one bending cycle represents the NFO-QDs bends by 45º with a bending curvature of 0.05 mm^{-1} and returns to its original location. As we can see, the NFO-PQDs after 1000 bending cycles demonstrate a slight change of emission intensity so that the lasing performance remained unchanged and the flexible NFO-PQDs are stable over many bending cycles. The main reason for the stability of using Ni foam as a substrate over the other organic substrate is metal in general stronger than organic materials as well as the well-controlled structure.

2.6. NFO-PQDs for speckle-free laser imaging

The high luminescence efficiency of lasers can be used as ideal light sources in optical imaging systems. However, the strong coherence of lasing light causing a 'speckle' problem (i.e. interference patterns of high spatial coherence light), which limits the corresponding quality of images. Fortunately, the emission characteristics of random lasers, which have a low spatial coherence of lasing light, can produce a speckle-free optical image.[31] **Figure 7a** shows an experimental setup for the use of NFO-PQDs as a laser source to produce a speckle-free optical image. Figures 7b and 7c compare the illuminated images obtained from using a commercial green laser and our NFO-PQDs respectively as the light sources. As shown in Figure 7b, laser speckles appear from the resolution test pattern under green laser illumination. On the other hand, sharp images are observed from the CCD under the as-prepared NFO-PQDs illumination

(Figure 7c). These results indicate that our as-prepared NFO-PQDs can provide low spatial coherence light which finds applications in the modern imaging systems as a flexible light source.

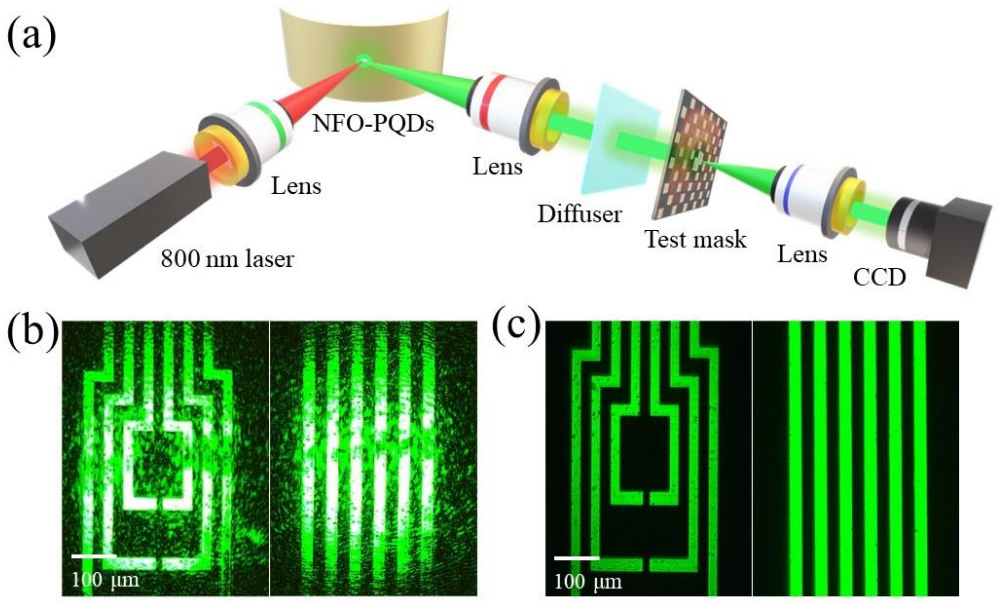

Figure 7. Optical imaging of micro-size patterns via a commercial laser and our as-prepared NFO-PQDs at room temperature. (a) Schematic diagram of the experimental setup for speckle-free imaging using the as-prepared NFO-PQDs as the illumination source. (b) The speckle image was generated from a commercial laser with a wavelength of 530 nm. (c) The speckle-free image was obtained by the as-prepared NFO-PQDs.

Recently, lasing sources with low spatial and spectral coherence have been proposed to generate speckle-free imaging such as broadband fiber sources,[32] broad-area VCSELs,[33] and surface-emitting random laser.[34] Alternatively, we can also use coherent lasers integrated with diffusers (i.e. to reduce light coherence) to produce speckle-free imaging.[35] **Table 1** summarizes the speckle-free imaging performance of various light sources. We compare their 'speckle contrast' or '*C*' (i.e. *C*= 0, no coherence, *C*=1 100% coherent light), 'contrast-to-noise ratio' or 'CNR' (i.e. the higher the better the image quality), maximum output power, and the complexity & cost or '*C*&*C*' for the fabrication of the lasing sources. It is noted that our flexible laser is as good as or better than that reported in the literature. More importantly, our metallic

substrate, which has high thermal conductivity, is an advantage over the other flexible light sources.

Table 1. Summary of the speckle-free imaging performance of various light sources.

Light source	Board-band fiber	Broad-area VCSELs	Coherent laser + diffuser	Surface random laser	Our random laser
C	≤ 0.02	≤ 0.19	< 0.22	< 0.01	< 0.01
CNR	≥ 1.0	≥ 1.0	≥ 1.2	≥ 1.5	≥ 1.5
Power	medium	low	high	low	low
C*&*C	medium	high	medium	medium	low
Ref	[32]	[33]	[35]	[34]	This work

3. Conclusions

In conclusion, we verified the possibilities to realize random lasers by deposition of PQDs via spin coating onto the flexible Ni foam. Incoherent random lasing is observed from the NFO-PQDs under two-photon excitation at room temperature. We also noted that the surface morphologies of the Ni foam determine the lasing characteristics of the NFO-PQDs and can be tuned by deforming the Ni foam. Flatted surface of Ni foam can only support ASE from the NFO-PQDs. On the other hand, the presence of the voids of the Ni foam supports incoherent random lasing and the corresponding lasing threshold is dependent on the size of the voids. More importantly, due to the flexibility and bending durability of the Ni foam, random lasing characteristics of the NFO-PQDs can be sustained over a long bending cycle without significant reduction of emission intensity. The advantage of incoherent random lasing is also demonstrated by using NFO-PQDs as the illumination light source to achieve ‘speckle’ free optical imaging. Hence, we have demonstrated the fabrication of random lasers on flexible metallic substrates and this is a stepping stone for the future development of high-performance speckle-free flexible lasing sources.

4. Experimental Section

4.1. Chemicals and Materials

Cesium carbonate (99%) (Cs_2CO_3), Oleic acid (AR) (OA), octadecene (ODE), oleylamine (80%-90%) (OAm), lead bromide (99%) ($PbBr_2$), and methyl acetate (98%) were purchased from Shanghai Aladdin Biochemical Technology Co., Ltd. Toluene was purchased from Sigma-Aldrich, Inc. All chemicals were used without further purification. The Ni porous foam was purchased from Kunshan Xingzhenghong Electronic Materials Co., Ltd., with the size of about 0.3 mm × 200 mm × 500 mm.

4.2. Synthesis of CsPbBr3 QDs

$CsPbBr_3$ PQDs were synthesized via the method proposed by Protesescu *et al*[20] with a slight modification. A mixture of Cs_2CO_3 (0.4 g), OA (1.25 mL), and ODE (15 mL) stirred under argon flow in a four-neck flask at 130 °C for about 10 min, and then raised the temperature to 150 °C until Cs_2CO_3 was completely reacted with OA and dissolved in the mixture. The mixture cooled down to room temperature, and this prepared Cs-precursor was stored in the glove box for further use. Another mixture of ODE (15 mL), OA (1.5 mL), OAm (1.5 mL), and $PbBr_2$ (0.2 g) was stirred under nitrogen at 130 °C for about 1 h. Then the temperature was raised to 180 °C after the $PbBr_2$ was completely dissolved and stirred for more than 10 min. Next, the Cs-precursor (1.5 mL) was injected into the above hot mixture as fast as possible, and the reaction stopped 5 s later with an ice bath. The reaction solution was centrifuged, and the precipitate was removed. The $CsPbBr_3$ QDs were precipitated from the supernatant after adding the methyl acetate, and the mixture was centrifuged at 13,000 rpm for 6 min to obtain the $CsPbBr_3$ QDs. The $CsPbBr_3$ QDs were washed by toluene and methyl acetate several times, and they were dispersed in toluene as a stable solution to deposit on the Ni foam.

4.3. Material Characterizations

Transmission electron microscopy (TEM) was carried out on a JEM-2100 electron microscope, operating at an acceleration voltage of 100 kV. Scanning transmission electron microscopy

(STEM) was carried out on a JEM-2100F field-emission electron microscope, operating at an acceleration voltage of 200 kV. SEM (scanning electron microscopy) images are captured with a JEOL Field Emission SEM. X-ray diffraction (XRD) patterns were acquired with a Bruker AXS D2 phaser X-ray diffractometer equipped with a Cu Kα radiation source (λ = 1.54 Å) at 40 kV and 30 mA. Absorption spectra and reflectance spectra were obtained on a PerkinElmer UV-vis-NIR spectrometer.

4.4. PL Measurement via Two-photon Excitation

A Ti:sapphire femtosecond laser (Coherent Libra), which generates femtosecond pulses (50 fs, 1 kHz) at 800 nm, was used as the excitation source. The laser beam, which has a diameter of ~8 mm, was focused onto the surface of the samples to an excitation beam of diameter ~200 μm by a convex lens of 10 cm focal length. The light emitted from the surface of the samples was collected by an objective lens (20 × 0.8 NA objective lens) and coupled to a conventional charge-coupled device (CCD) camera for the recording of the near-field image or attached to a monochromator (Princeton SpectraPro 2750 integrated with a ProEM EMCCD camera with a spectral resolution less than 0.1 nm) for spectrum analysis.

Supporting Information

Supporting Information is available from the Wiley Online Library or the author.

Acknowledgments

This work was supported by the National Natural Science Foundation of China (Grant No. 61775187) and The Hong Kong Polytechnic University grants (Grant Nos. 1-BBA5, G-YBHG, 1-ZVGH, and BCEE)

Conflict of Interest

The authors declare no conflict of interest.

Received: ((will be filled in by the editorial staff))
Revised: ((will be filled in by the editorial staff))
Published online: ((will be filled in by the editorial staff))

References

1. Hu, J.; Li, L.; Lin, H.; Zhang, P.; Zhou, W.; Ma, Z., Opt. Mater. Express 2013, 3 (9), 1313-1331.
2. Lee, Y.-J.; Chou, C.-Y.; Yang, Z.-P.; Nguyen, T. B. H.; Yao, Y.-C.; Yeh, T.-W.; Tsai, M.-T.; Kuo, H.-C., Nanoscale 2018, 10 (22), 10403-10411.
3. Ali, T.; Lin, J.-D.; Snow, B.; Wang, X.; Elston, S. J.; Morris, S. M., Advanced Optical Materials 2020, 8 (8), 1901891.
4. Li, X.; Liu, H.; Xu, X.; Yang, B.; Yuan, H.; Guo, J.; Sang, F.; Jin, Y., ACS Applied Materials & Interfaces 2020, 12 (8), 10050-10057.
5. Wang, Z.; He, H.; Liu, S.; Wang, H.; Zeng, Q.; Liu, Z.; Xiong, Q.; Fan, H. J., Small 2020, 16 (43), 2004409.
6. Lau, S. P.; Yang, H.; Yu, S. F.; Yuen, C.; Leong, E. S.; Li, H.; Hng, H. H., Small 2005, 1 (10), 956-9.
7. Kim, J.-H.; Inoue, M.; Zhao, L.; Komino, T.; Seo, S.; Ribierre, J.-C.; Adachi, C., Applied Physics Letters 2015, 106 (5), 053302.
8. Karl, M.; Glackin, J. M. E.; Schubert, M.; Kronenberg, N. M.; Turnbull, G. A.; Samuel, I. D. W.; Gather, M. C., Nature Communications 2018, 9 (1), 1525.
9. Wang, Y. C.; Li, H.; Hong, Y. H.; Hong, K. B.; Chen, F. C.; Hsu, C. H.; Lee, R. K.; Conti, C.; Kao, T. S.; Lu, T. C., ACS Nano 2019, 13 (5), 5421-5429.
10. da Silva-Neto, M. L.; de Oliveira, M. C. A.; Dominguez, C. T.; Lins, R. E. M.; Rakov, N.; de Araújo, C. B.; Menezes, L. d. S.; de Oliveira, H. P.; Gomes, A. S. L., Scientific Reports 2019, 9 (1), 11765.
11. Liang, J.; Chen, D.; Yao, X.; Zhang, K.; Qu, F.; Qin, L.; Huang, Y.; Li, J., Small 2020, 16 (15), 1903398.
12. Liu, X.; Yu, D.; Song, X.; Zeng, H., Small 2018, 14 (36), 1801460.
13. Gao, W.; Yu, S. F., EcoMat 2021, 3 (1).
14. Jin, M. F. F.; Gao, W.; Liang, X. J.; Fang, Y.; Yu, S. F.; Wang, T.; Xiang, W. D., Nano Research 2021.
15. Zhao, Y.; Li, J.; Dong, Y.; Song, J., Israel Journal of Chemistry 2019, 59 (8), 649-660.
16. Chen, D.; Chen, X., Journal of Materials Chemistry C 2019, 7 (6), 1413-1446.
17. Xiao, M.; Hao, M.; Lyu, M.; Moore, E. G.; Zhang, C.; Luo, B.; Hou, J.; Lipton-Duffin, J.; Wang, L., Advanced Functional Materials 2019, 29 (48), 1905683.
18. Li, S.; Lei, D.; Ren, W.; Guo, X.; Wu, S.; Zhu, Y.; Rogach, A. L.; Chhowalla, M.; Jen, A. K., Nat Commun 2020, 11 (1), 1192.
19. Li, X.; Cao, F.; Yu, D.; Chen, J.; Sun, Z.; Shen, Y.; Zhu, Y.; Wang, L.; Wei, Y.; Wu, Y.; Zeng, H., Small 2017, 13 (9), 1603996.
20. Protesescu, L.; Yakunin, S.; Bodnarchuk, M. I.; Krieg, F.; Caputo, R.; Hendon, C. H.; Yang, R. X.; Walsh, A.; Kovalenko, M. V., Nano Letters 2015, 15 (6), 3692-3696.
21. Wang, Y.; Li, X.; Song, J.; Xiao, L.; Zeng, H.; Sun, H., Adv Mater 2015, 27 (44), 7101-8.
22. Cao, X.; Zhi, L.; Jia, Y.; Li, Y.; Zhao, K.; Cui, X.; Ci, L.; Zhuang, D.; Wei, J., ACS Applied Materials & Interfaces 2019, 11 (8), 7639-7654.
23. Yang, Z.; Zhang, S.; Li, L.; Chen, W., Journal of Materiomics 2017, 3 (4), 231-244.
24. Zheng, K.; Zheng, C.; Zhang, Y.; Wang, Y.; Tittel, F. K., Sensors (Basel) 2018, 18 (11), 3646.
25. Sznitko, L.; Cyprych, K.; Szukalski, A.; Miniewicz, A.; Mysliwiec, J., Laser Physics Letter 2014, 11, 045801.
26. Gummaluri, V. S.; Gayathri, R.; Vijayan, C.; Murukeshan, V. M., Journal of Optics 2020, 22 (6), 065003.
27. Cao, H., Waves in Random Media 2003, 13 (3), R1-R39.

28. Yu, S. F.; Yuen, C.; Lau, S. P.; Park, W. I.; Yi, G.-C., Applied Physics Letters 2004, 84 (17), 3241-3243.
29. Burin, A. L.; Cao, H.; Ratner, M. A., Physica B: Condensed Matter 2003, 338 (1), 212-214.
30. Berestennikov, A. S.; Li, Y.; Iorsh, I. V.; Zakhidov, A. A.; Rogach, A. L.; Makarov, S. V., Nanoscale 2019, 11 (14), 6747-6754.
31. Redding, B.; Choma, M. A.; Cao, H., Nat Photonics 2012, 6, 355-359.
32. Redding, B.; Ahmadi, P.; Mokan, V.; Seifert, M.; Choma, M. A.; Cao, H., Opt. Lett. 2015, 40 (20), 4607-4610.
33. Riechert, F.; Verschaffelt, G.; Peeters, M.; Bastian, G.; Lemmer, U.; Fischer, I., Optics Communications 2008, 281 (17), 4424-4431.
34. Liu, Y.; Yang, W.; Xiao, S.; Zhang, N.; Fan, Y.; Qu, G.; Song, Q., ACS Nano 2019, 13 (9), 10653-10661.
35. Kumar, V.; Kumar Dubey, A.; Gupta, M.; Singh, V.; Butola, A.; Singh Mehta, D., Optics & Laser Technology 2021, 141, 107079.

Metal foams can be used as the substrates of flexible random lasers due to their well-controlled configuration. Herein, metal halide perovskites quantum dots are coated onto nickel foams to realize flexible random lasers with tunable lasing characteristics by the deformation of the 3D nickel foams. This flexible laser is a potential light source for application in speckle-free lasing imaging.

Wei Gao, Ting Wang, Jiangtao Xu, Ping Zeng, Wenfei Zhang, Yunduo Yao, Changsheng Chen, Mingjie Li, Siu Fung Yu*

Robust and flexible random lasers using perovskite quantum dots coated Nickel foam for speckle-free laser imaging

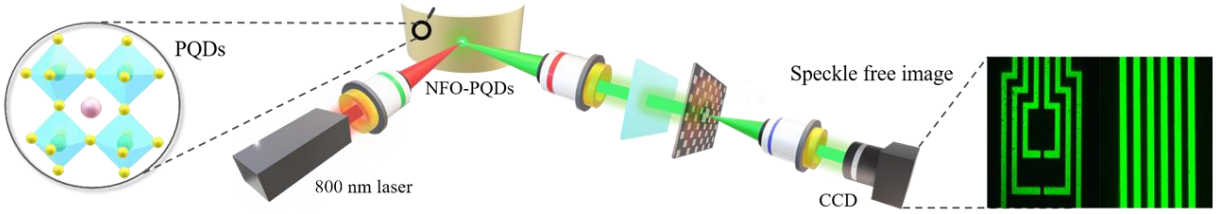

Supporting Information

Robust and flexible random lasers using perovskite quantum dots coated Nickel foam for speckle-free laser imaging

*Wei Gao, Ting Wang, Jiangtao Xu, Ping Zeng, Wenfei Zhang, Yunduo Yao, Changsheng Chen, Mingjie Li, Siu Fung Yu**

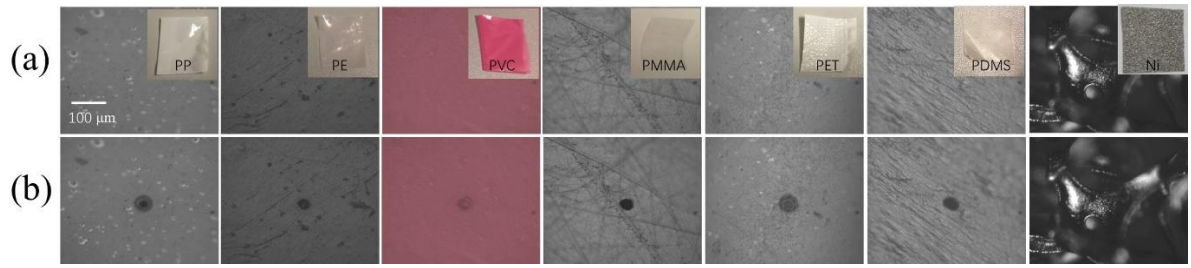

Figure S1. Microscope images of flexible plastic samples (PP, PE, PVC, PMMA, PET, PDMS) and Ni foam (last sample on the right) (a) before and (b) after 5 seconds 800 nm fs laser radiation at 220 μJ/cm^2 with a beam diameter of ~200 μm. All plastic samples are burnt by the laser due to thermal effect, while the Ni foam remains intact.

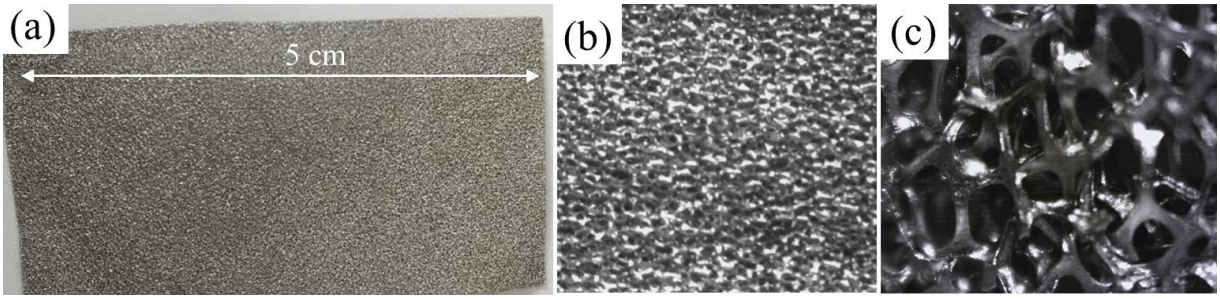

Figure S2. Photos of the Ni foam, which voids have a diameter of ~200 μm, are taken by CCD with (a) 1×, (b) 100× and (c) 1000× magnification.

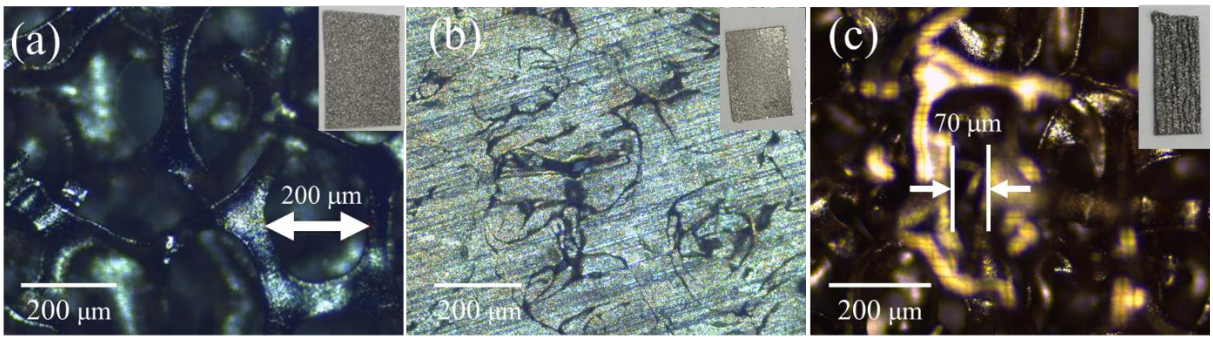

Figure S3. The microscope images of (a) original Ni foam with the void diameter of ~100 – 200 µm, (b) flat Ni foam is obtained due to vertical compression applied to the surface of the Ni foam, and (c) horizontal compression applied to the surface of the Ni foam so that the diameter of the voids reduce to ~60 – 90 µm, as a result, the number of scatterers per unit length is increased. The insets are the photo of the samples.

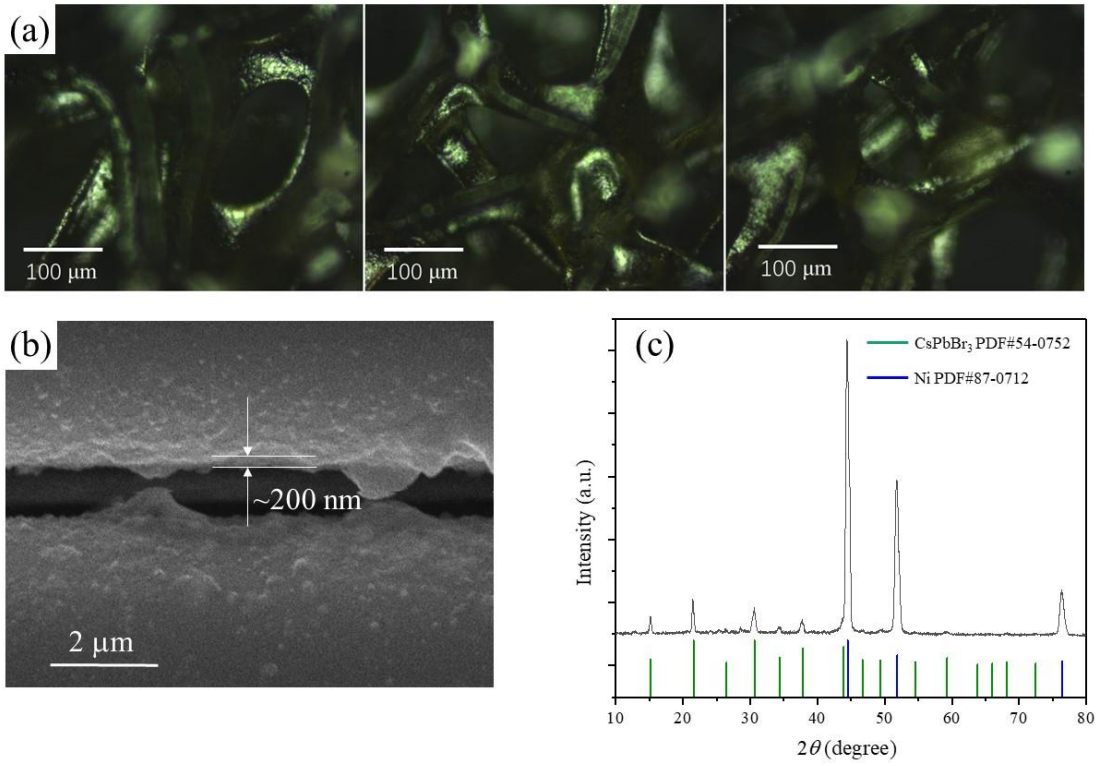

Figure S4. (a) Three optical microscope images of the surface of the NFO-PQDs. (b) Cross-section SEM image of the NFO-PQDs. The PQDs coating on the Ni foam has an average thickness of ~200 nm. (c) XRD pattern of PQDs coated Ni porous foam. The XRD pattern well matches with that of the $CsPbBr_3$ (green color) and Ni (blue color).

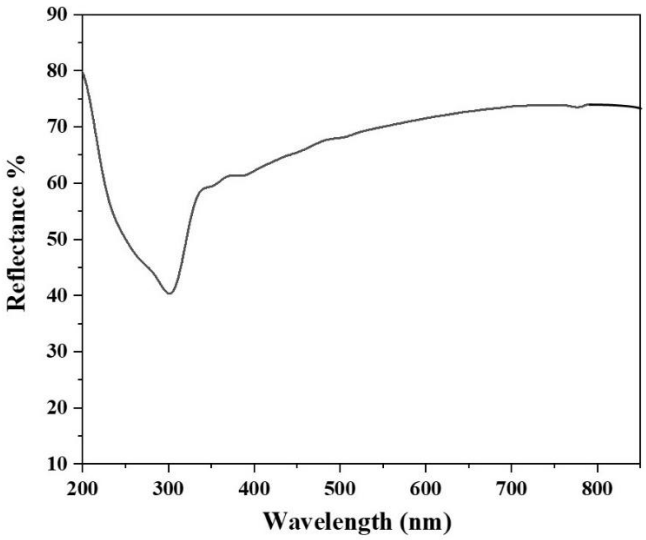

Figure S5. The reflection spectrum of the surface of the flattened Ni foam.

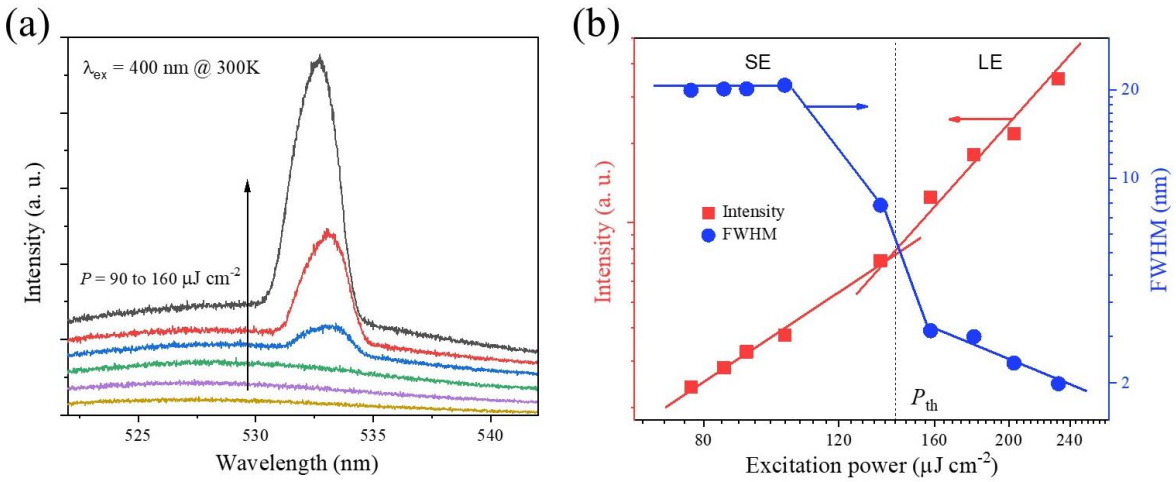

Figure S6. Room temperature emission characteristics of NFO-PQDs under fs laser excitation at 400 nm. 400 nm fs laser light is generated via a BBO crystal through second-harmonic generation from 800 nm fs laser light. The NFO-PQDs used here are identical to that of Figure 3. (a) Emission PL spectra measured at different excitation power. (b) Output intensity and linewidth at various excitation power. As the NFO-PQDs only demonstrate ASE, 400 nm excitation wavelength is less efficient to support random lasing action on the Ni foam.

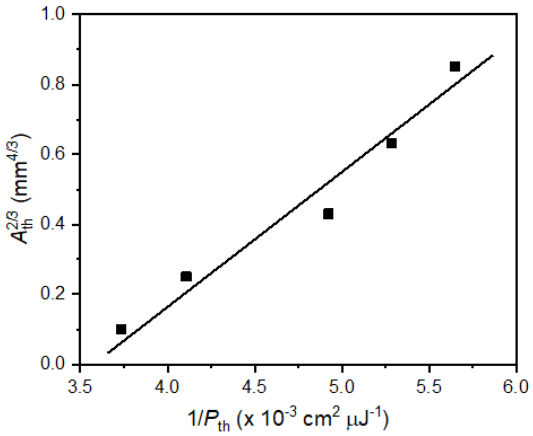

Figure S7. Plot of $A_{th}^{2/3}$ versus 1/P_{th} for the NFO-PQDs.

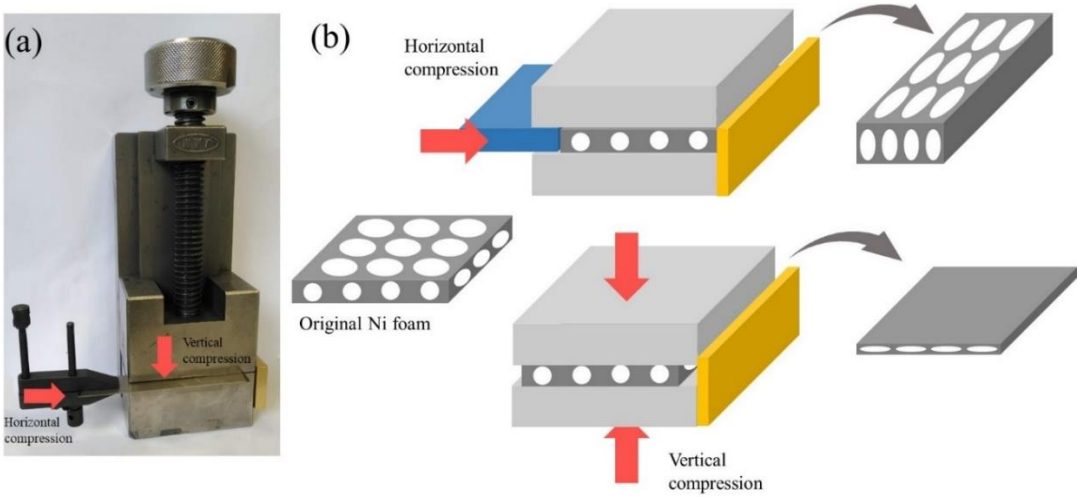

Figure S8. (a) The device used to apply vertical and horizontal compression to deform the Ni foam. (b) Schematic diagram to explain how the vertical and horizontal compressions are applied to deform the mesh structure of the Ni foam.

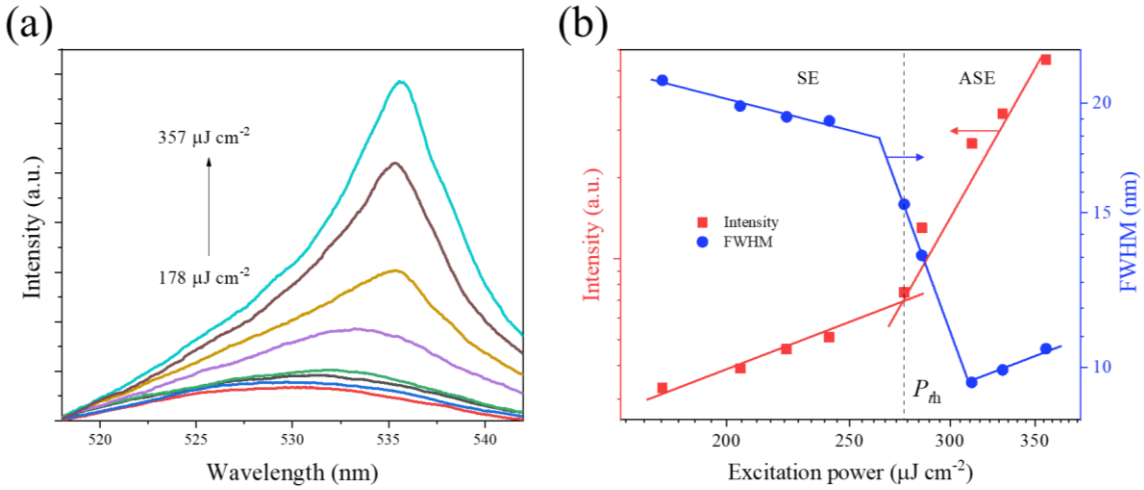

Figure S9. (a) PL spectra and light-light curve of $CsPbBr_3$ QDs coated on flat Ni ribbon with the smooth surface under various excitation power. The thickness of $CsPbBr_3$ QDs is similar to that shown in Figure 3.

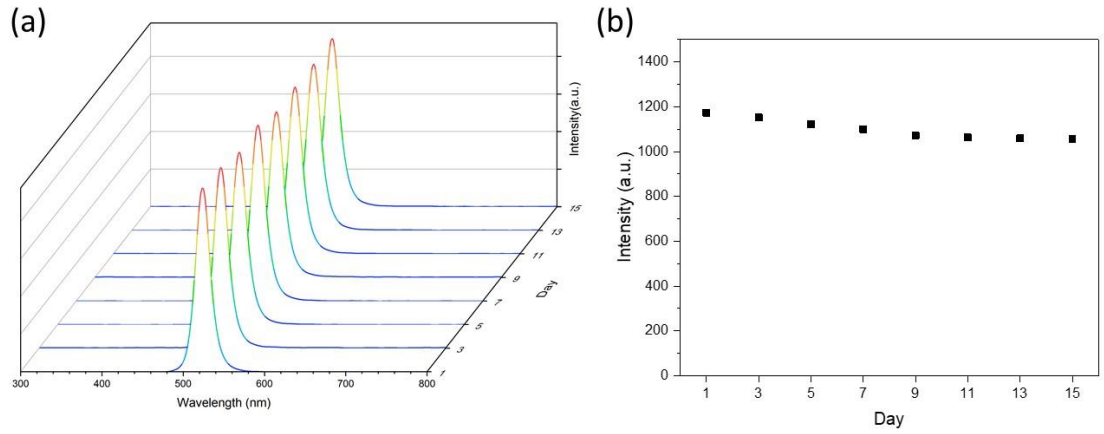

Figure S10. Stability analysis of $CsPbBr_3$ QDs coated on Ni foam which is similar to that given in Figure 3. (a) PL spectra of the QDs on Ni foam for 15 days under a constant power excitation at ~160 μJ cm^{-2}. (b) The corresponding peak intensity of the PL spectra shown in part (a). The sample, which was left at room temperature with humidity control, was excited every day to measure the corresponding emission characteristics.